Results in Engineering 23 (2024) 102543

Contents lists available at ScienceDirect

Results in Engineering

journal homepage: www.sciencedirect.com/journal/results-in-engineering

# Experimental and numerical study of a linear Fresnel solar collector attached with dual axis tracking system

Qusay J. Abdul-Ghafoor, Sundus Huseein Abed, Saif Ali Kadhim *, Mustafa A. Al-Maliki

*Mechanical Engineering Department, University of Technology- Iraq, Baghdad, 10066, Iraq*

ARTICLE INFO

*Keywords:*
Linear Fresnel collector
Thermal efficiency
Exergy efficiency
Tracking system
CFD

ABSTRACT

The demand for an alternative to fossil fuel energy is increasing as environmental and economic challenges rise. The linear Fresnel solar collector is considered a promising option for obtaining thermal energy at medium and high temperatures. A linear Fresnel solar collector consists of a number of mirror strips that are used to focus solar beam radiation toward a line receiver. This study aims to obtain a clear evaluation of the thermal performance of a linear Fresnel solar collector through design, manufacture, and experimental testing under different outdoor conditions in Baghdad over various periods. There have been tests on April 1 and 22, as well as May 8 and 27, using water as the working fluid. The solar collector used is an aluminum base measuring 200 cm in length and 150 cm in width on which 14 mirror strips from each side are fixed. The receiver (absorber copper tube) has a length of 200 cm and a height of 60 cm from the base. The solar collector is provided with a dual-axis tracking system (North-South and East-West) for ensuring that the solar concentrator faces the sun at normal incidence during all daytime hours. The best thermal performance of the solar collector was observed on May 27, where the average useful energy, thermal and exergy efficiency reached 1042.61 W, 39.15 %, and 1.31 %, respectively. The present study also included a numerical analysis done using computational fluid dynamics (CFD) to verify the experimental results. The numerical results confirmed the validity of the experimental results.

Nomenclature

| Symbol | | | |
|---|---|---|---|
| $A$ | Aperture area ($m^2$) | $\theta$ | Incident angle (deg.) |
| $C$ | Specific heat of water (kJ/kg.$^o$C) | $\mu$ | Viscosity (N.s/$m^2$) |
| $E$ | Exergy rate (W) | $\rho$ | Density (kg/$m^2$) |
| $e_R$ | Relative error | $\eta$ | Efficiency |
| $G$ | Solar radiation (W/$m^2$) | **Subscripts** | |
| $g$ | Gravity acceleration (m/$s^2$) | $a$ | Ambient |
| $\dot{m}$ | Mass flow rate (kg/s) | $av$ | Average |
| $Q$ | Energy rate (W) | $b$ | Beam |
| $T$ | Temperature ($^o$C) | $ex$ | Exergy |
| $u$ | Velocity in the $x$ direction (m/s) | $i$ | Inlet |
| $v$ | Velocity in the $y$ direction (m/s) | $o$ | Outlet |
| $w$ | Velocity in the $z$ direction (m/s) | $s$ | Solar |
| **Greeks symbol** | | $th$ | Thermal |
| $\varnothing$ | The angle between incident and reflected beam (deg.) | $w$ | Water |

## 1. Introduction

Solar energy is harnessed to produce thermal energy in several applications such as solar stills for evaporating water [1,2], solar cookers for cooking food [3,4], solar dryers for drying fruits and vegetables [5,6], solar air heaters for heating homes [7,8], and solar collectors of various types for heating water [9–12]. One of the concentrating type solar collectors with a significant potential for thermal usage is the linear Fresnel reflector, also known as the linear Fresnel solar collector or linear Fresnel concentrator. It consists of a family of mirror rows fixed on a metal frame at calculated angles for reflecting the normal solar radiation toward the absorber tube, which is fixed in the focal line of the collector. Through the absorber tube, the concentrated solar power is delivered to the working fluid and a useful power was accomplished as a consequence of flow temperature rise. The Fresnel concentrator with its accessories are shown in Figure (1) [13]. The linear Fresnel reflector technology has a variety of uses. Small-scale linear Fresnel reflectors are utilized in the construction industry as opposed to large-scale linear Fresnel reflectors, which are employed in the production of energy and

* Corresponding author.
*E-mail address:* 20096@uotechnology.edu.iq (S.A. Kadhim).

https://doi.org/10.1016/j.rineng.2024.102543
Received 14 May 2024; Received in revised form 25 June 2024; Accepted 9 July 2024
Available online 9 July 2024

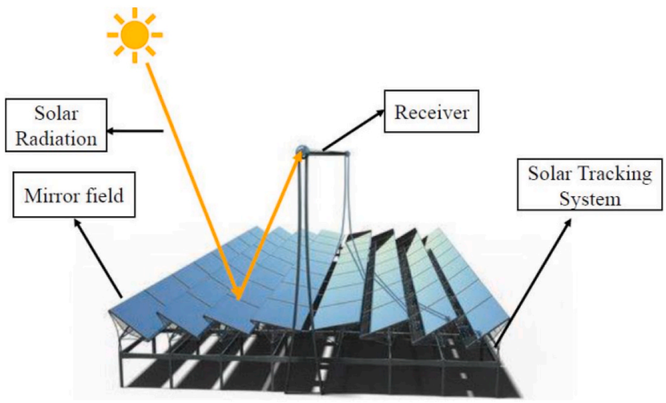


**Figure 1.** Linear Fresnel solar collector.

industrial operations [14–19]. The incidence angle of solar irradiance on the receiver tube will be determined in two projection planes [20]: the transversal incidence angle and the longitudinal incidence angle, taking into account a linear Fresnel reflector oriented in a North-South direction. The secondary reflector focuses sunlight toward the absorber tube in the transverse plane. Various secondary reflector designs, including compound parabolic designs, involute designs, parabolic designs [21, 22], butterfly designs, trapezoidal designs, triangle designs, and other complex geometries, have been presented over the past few years. Not all of the solar rays are reflected by the mirrors in the longitudinal plane land on the absorber tube [23–26].

End losses are the results of this phenomenon [27]. However, some of the solar rays are reflected by the mirrors and do not hit the absorber tube. The latitude of the site, the moment of evaluation, and the geometry of the mirrors' field all affect the absorber tube's end losses [28]. The rows of mirrors and the absorber tube in a large-scale linear Fresnel reflectors have an angle of 0° with the horizontal plane. Additionally, the absorber tube and the rows of mirrors lack longitudinal movement because of their sizes. In this instance, the rows of mirrors can be turned around on a North-South axis to track the daily motion of the Sun (transversal movement). In this reflector, the end loss efficiency is approximately 97 percent as a result of the size of the absorber tube and the height of the receiver, in Almeria (Spain) [29], and the loss of reflected light is typically not taken into account in the mathematical expression usually used to calculate the power absorbed by the absorber tube [27,30,31]. The configurations of longitudinal movements are numerous. Rows of mirrors may move continually throughout the day or only once throughout the day. In the first set of configurations, the design makes sure that the longitudinal radiation reflected by the mirrors are always normal to the absorber tube, regardless of the time of day. The longitudinal inclination of the second set of configurations, after declination adjustment, is equal to the location's latitude. Additionally, the secondary reflector might move longitudinally in a similar manner to the rows of mirrors. In other arrangements, the secondary reflector system does not have longitudinal movement and instead forms a certain angle with the horizontal plane. All of these setups can be used with the new solar tracking that is being offered.

Some studies have focused on verifying the performance of a linear Fresnel solar collector, whether thermally, optically, or flow analysis. Additional research has been conducted on the designs of this collector to improve its efficiency, whether it is about reflectors, receivers, or both. Other studies have used hybrid systems by combining this collector with other application(s). Moreover, not only water, other fluids such as Nano-fluids have been used as working fluids to enhance performance. There are also studies aimed at reducing optical losses, or so-called end losses, common in Fresnel liner reflectors through various techniques, including two-axis tracking. Some studies are highlighted in the next paragraph.

Bellos et al. [32] presented a numerical and experimental study to evaluate the performance of a linear Fresnel solar collector with flat plate receiver. They developed an innovative model to determine the optical, energy and exergy performance of the collector in various operating conditions. The model was validated using the respective experimental data. Water was considered as a working fluid and also oil is used (in simulation only). Their results showed that this solar collector is capable of producing approximately 8.5 kW of useful power in the summer, 5.3 kW in the spring, and 2.9 kW in the winter. Furthermore, operating this solar collector with oil can produce satisfactory results up to 250 °C. Bellos and Tzivanidis [33] presented an innovative model to enhance the thermal performance of the linear Fresnel solar collector in the high temperature range using CuO nanoparticles scattered on Syltherm 800 (6 % concentration by volume). The results of the Nano-fluid were compared with thermal oil for different inlet temperatures ranging from 77 °C to 377 °C and a flow rate equals to 200 l/min. According to their results, the maximum thermal efficiency enhancement using Nano-fluid is near to 0.8 %. It also turns out that the process using Nano-fluid is beneficial, especially at high temperature levels after applying various parameters such as the overall efficiency and exergy efficiency. Dabiri et al. [34] analyzed the rate of heat transfer loss in a trapezoidal cavity of the linear Fresnel solar collector concentrator using discrete transfer radiation model (DTRM) for the simulation. The effect of the cavity angle and the tubes size are evaluated on the performance of the collector. Their results show that with increasing cavity angle, the overall value of the heat transfer rate increases, but the absorbed energy by each tube decreases, and that the effect of tube size on heat transfer rate is less, compared to the cavity angle effect. Ghodbane et al. [35] evaluated the thermal performance of linear Fresnel solar reflector with trapezoidal cavity using multi-walled carbon nanotubes (MWCNTs) dispersed in distilled water (DW) with the volume fractions of 0.05 %, 0.1 % and 0.3 % and compared to DW. They developed a one-dimensional model to determine the unsteady behavior of the Nano-fluid within the linear solar reflector and the numerical model is validated with experimental results. Their results showed that MWCNTs/DW Nano-fluid with 0.3 % volume ratio has the highest thermal efficiency of 33.8 % and the lowest entropy generation but at the same time it is noted increase in pressure loss. Beltagy [36] studied the influence of glass cover on the receiver and also the use of two absorber tubes on optical performance of linear Fresnel solar concentrator by a modeling and numerical simulation. The results show that the removal of the glass results in an increase of annual optical efficiency up to 5.6 % and the use of two absorber tubes led to increase in optical efficiency estimated at 15.5 %. Montes et al. [37] presented a thermal design for the multi-tube receiver linear Fresnel solar collector based on three facts that have to be considered for any multi-tube receiver: the fluid flow layout is arranged to correspond to the symmetry of the solar intensity map. The fluid circulates from the lower to the higher density region. The fluid velocity is amended by modifying the diameter of the tube to improve the heat transfer. According to these facts, the final shape of the receiver is chosen based on the exergy optimization. Hasan et al. [38] conducted simulation using the finite volume method to demonstrate the effect of inserting the transverse ribs inside the receiver tube of the linear Fresnel solar collector system boosted with upturned compound parabolic collector (CPC) on the thermal and flow performance parameters. Water is used as the working fluid, at Reynolds numbers ranging 5000 to 13000, and this tube is compared with the conventional absorber tube. Their results showed that the average Nusselt number in the absorber tube with ribs is greater than that in the conventional absorber tube, and the skin friction coefficient of the absorber tube with ribs is larger than that in the conventional absorber tube, at all Reynolds numbers. Zhang et al. [39] suggested a new linear Fresnel solar concentrator system as two small experimental systems were created according to the design principle (flat and cylindrical focal plane reception) with low cost. Monocrystalline silicon cells and a double-tube heat collector are placed as receivers. Their experimental results showed that for a flat focal plane receiving system, this type of condenser can obtain the focus point with a uniform distribution of intensity on the focal plane. They found that monocrystalline silicon cells have high generation efficiency after testing the voltammetric characteristics, and in case of heat collector, with two collector tubes connected in series, the experimental photothermal conversion efficiency reaches about 0.74. They recommended that this type of concentrator can be widely used in photovoltaic and photothermal applications due to low cost and good concentrating performance. Cucumo et al. [40] obtained a mathematical law to analytically determine the position that each reflector should take during the day in order to reduce the energy losses (end losses) in linear Fresnel solar concentration systems. Their study showed that the reflector must be moved independently in each direction. They also studied a configuration in which the reflectors are moved around an axis with the same motor in order to reduce the cost, they showed that the tracking error committed is not significant, thanks to the presence of the secondary reflector. Yang et al. [41] designed and analyzed a simple mechanical dual-axis tracking system and connected it with a linear Fresnel reflector with the aim of reducing end losses or optical losses. They placed a Linear Fresnel reflector with east-west rotational tracking on north-south rails and driven by a linear actuator. The idea is to eliminate end losses when the reflector slides along the rails while keeping the receiver fixed. According to the results of the experimental and simulation analyses of the designed system's performance, the collector length and latitude can affect the annual average optical efficiency of a linear Fresnel reflector by 8–50 %. In order to improve the optical performance of a linear Fresnel reflector with north-south orientation, Bellos et al. [42] presented three novel techniques to reduce the optical end losses. The first technique is the extension of the receiver after the concentrator, the second one is the displacement of the receiver in order to eliminate the non-illuminated area at the beginning of the receiver, and the third is the hybrid design, which combines the extended and displayed receiver. According to their results, the first technique enhances the annual mean incident angle modifier up to 50.3 %. The second one also enhances the mean annual incident angle modifier up to 20.2 % for a displacement that is equal to 20 % of the concentrator length. While the third one leads to intermediate enhancements compared to the previous cases, its advantage is the lower investment cost compared to the simple receiver extension case. Barbón et al. [29] designed a new open-loop solar tracking system for a small-scale linear Fresnel reflector with three movements. According to their results, this system gives 16.64 % more energy, a 78.46 % higher energy/area ratio, and a 4.62 % less cost of energy that the classic tracking system with one movement used in large scale linear Fresnel reflectors. In addition to what has been presented, there are many other relevant studies to verify or enhance performance of the linear Fresnel solar collector [43–48].

It is clear from the literature review that differences in design, choice of working fluid, and operating conditions greatly affect the performance of the linear Fresnel solar collector. It was observed that there are few studies on the use of a dual-axis tracking system to enhance the performance of these solar collectors. This paper presents an experimental and numerical analysis to evaluate the thermal performance of a linear Fresnel solar collector in the external conditions of Baghdad city. The solar collector is designed and manufactured with local materials readily available in the area and is supplemented by a dual-axis tracking system (East-West and North-South) consisting of two reasonably priced, low-power DC motors. The purpose of the dual-axis tracking system is to ensure that the greatest possible amount of solar radiation is reflected onto the absorber tube. Fresh water is used as the working fluid, and a solar collector is installed outdoors in order to conduct tests at different weather conditions. Then the experimental results are verified via the simulation of the system using CFD.

## 2. Experimental layout

### 2.1. Building up the model

The fundamental components prepared for the design and manufacture of the Linear Fresnel solar collector in this study are as follows: A metal stand on which the base is fixed. A metal frame with supports serves as the base. A mirror strip is attached to the base supports. A metal holder on which the receiver tube (absorber copper tube) is fixed. To guarantee that the solar collector moves in both the x and y directions, two DC motors are attached to the base and stand. **Figure (2)** provides design specifications for the linear Fresnel solar collector.

### 2.2. Design of the angle of the Fresnel collector mirror strips

The angles of the system's strips were determined by making the assumption that solar radiation strikes the system perpendicularly from where the incident beam reaches each strip at an angle of half their breadth. The tilt angle of the mirror strip must be computed so that the reflected beam strikes the receiver tube center. Assuming that the angle between the incident and reflected beams is ($\varnothing$). Accordingly, the angle of this strip is ($\theta = \varnothing/2$) and all other angles were computed in the same manner.

Details of each strip's design are displayed in Table (1). As seen in Figure (3), Auto CAD software was used to determine the angles of the strips based on their distance from the fixed receiver and the angle at which the sun will fall on them.

### 2.3. Materials and measuring devices

The stand is made of iron and has a dual-axis mechanism for operation. The mechanism of the tracking system is designed and fabricated on top of the stand. It consists of an iron shaft, a circular base, and a number of bearings that are fixed together by a number of screws and welded together until, it could build a shape with two harmonically moving axes. The frame (base of mirror strips) was designed from aluminum material with 200 cm length and a 50 cm width. The receiver (absorber copper tube) was at a height of 60 cm from the frame. The mirror slides were projected onto the frame (base) according to the locations and angles displayed in the previous table. Longitudinal glass mirror strips were chosen as the solar radiation reflectors. 14 mirror strips were used, each strip dimensions were 1.5 m length and 5 cm width. The reflectivity of the mirror strip was measured in a certified laboratory in the Ministry of Science and Technology. Its reflectivity value had found of 0.92 (That is, mirrors are able to reflect 92 % of the solar radiation falling on them), which is suitable to fulfill the required purpose. The mirror strips were fixed on supports of the metal base in such manner to reflect the solar radiation toward the receiver tube, as shown in Figure (4).

The receiver is a tube designed from copper material, because of its high thermal conductivity (383 $W/m^{2\circ}C$) and is widely available at an appropriate economic cost. The copper tube, measuring 1.5 m in length and 1.25 cm in diameter, was designed with a copper fin to trap solar radiation that did not strike the copper tube directly. For achieving the highest energy value, the copper tube was coated with a unique black paint. This paint absorbs the highest possible solar radiation that strikes on it and emits the fewest radiation. The available coating type was of 0.87 absorptivity and 0.2 emissivity values. Two plastic tanks were added, the first to store water entering the solar collector and the other to store water leaving the solar collector. Rubber hoses connect the receiver tube to the tanks, allowing the tracking system to freely move all of the system's assembled parts, including the copper receiver.

The tracking system control panel consists mainly of hardware and software; the hardware parts consist of two linear actuators "HARL3624 Super-Jack", its specifications are a bore length of (85) cm, operation at 36 DC volts, and maximum current of 3A. The actuator shaft linear

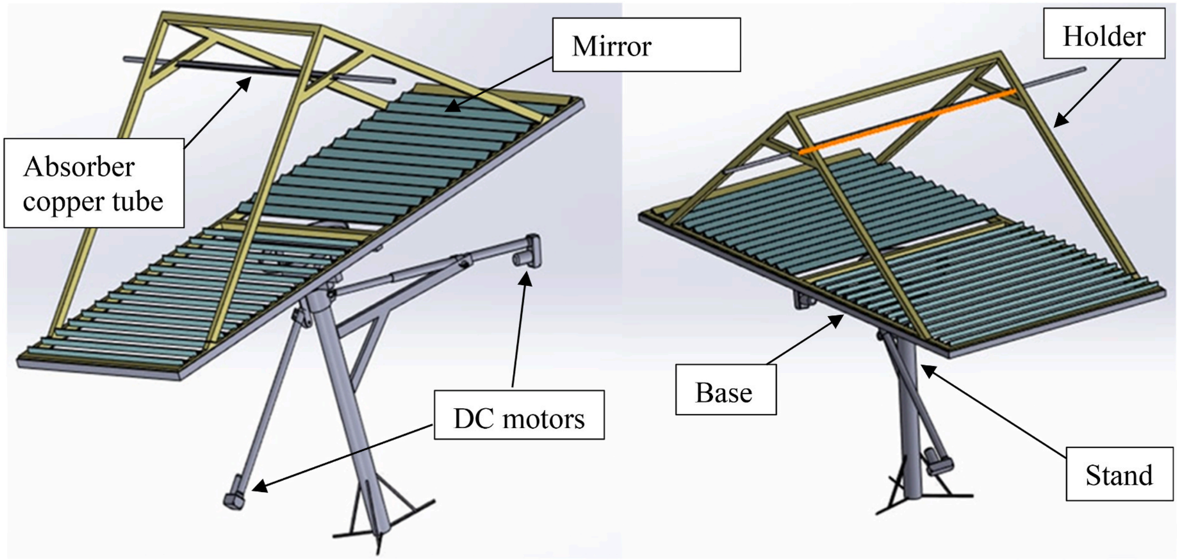


**Figure 2.** Linear Fresnel solar collector model.

**Table 1**
Details of the mirror strip's design angles.

| strip number (n) | The angle of reflection (∅) (deg.) | The angle of inclination strips (θ) (deg.) | The distance of each strip from the centers) L) (cm) | The beginning of each strip) P) (cm) |
|---|---|---|---|---|
| **1** | 5 | 2.5 | 5 | 0 |
| **2** | 9 | 4.5 | 10.0365 | 5.0135 |
| **3** | 14 | 7 | 15.1808 | 10.0369 |
| **4** | 19 | 9.5 | 20.3927 | 15.1808 |
| **5** | 23 | 11.5 | 25.7196 | 20.3927 |
| **6** | 27 | 13.5 | 31.1882 | 25.7196 |
| **7** | 51 | 15.5 | 36.8264 | 31.1882 |
| **8** | 35 | 17.5 | 42.6641 | 36.8264 |
| **9** | 38 | 19 | 48.7134 | 42.6641 |
| **10** | 42 | 21 | 55.0245 | 48.7134 |
| **11** | 45 | 22.5 | 61.6086 | 55.0245 |
| **12** | 48 | 24 | 68.4981 | 61.6086 |
| **13** | 51 | 25.5 | 75.7278 | 68.4981 |
| **14** | 53 | 26.5 | 83.2998 | 75.7278 |

velocity is about 5.6 mm/s, and it could withstand approximately 250 and 450 kg of dynamic and static loads, respectively. It is also equipped with a limit switch that is programmed to cut off the power so as to ensure that the moving path does not exceed the bore length. The microcontroller board of type "Arduino" Omega is programmed to control the movement of the linear actuators in the two axes. In addition, there is an LCD 6x2 I2C screen that shows the time and date in addition to data like flow level, solar radiation intensity, and entry and exit temperatures. Figure (5) displays all of the previously mentioned parts.

Measuring devices are also attached to the system. The water temperatures was measured by thermocouple type K. The achieved signal from the thermocouple was fed to Arduino microcontroller card. Also, the mass flow rate of the working fluid was measured by digital flow meter where its signal fed to the Arduino microcontroller card. Both temperatures and water flow rate data were attained from the attached digital display connected to the control system. During the test days, the solar radiation intensity is monitored using a solar power meter, the wind speed is monitored using an anemometer, and the ambient temperature is monitored using a mercury thermometer. Table (2) shows the ranges of measuring devices and their uncertainty and Figure (6) shows

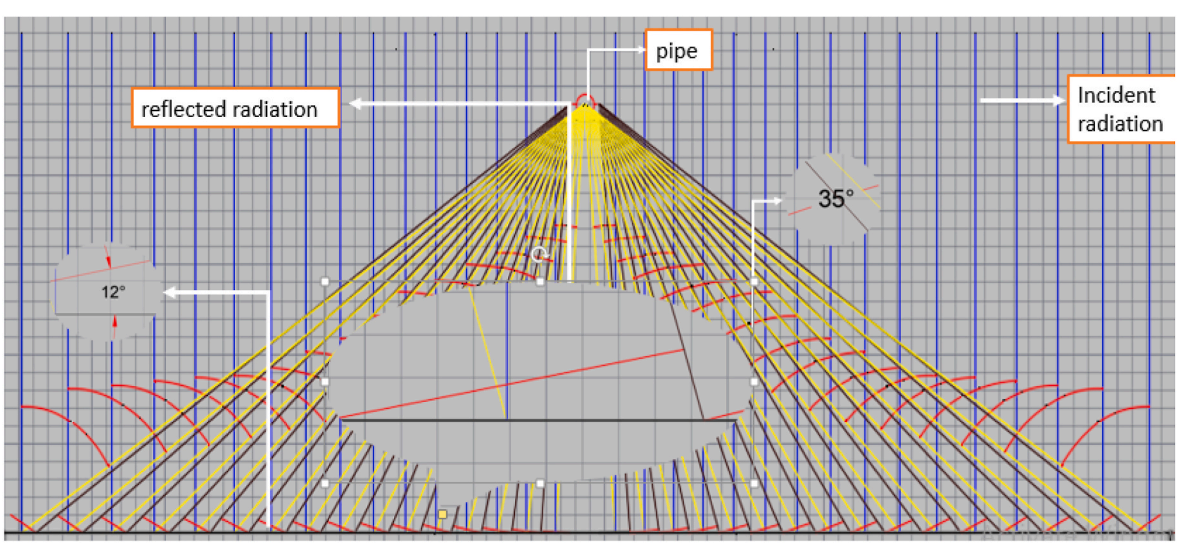


**Figure 3.** Mirror strips design angles.

**Figure 4.** Installing the mirror strips on the base supports.

a photograph of the linear Fresnel solar collector and all its accessories following the completion of design and manufacturing. It should be noted that the direct solar irradiance is measured by shade-unshaded technique under clear sky conditions with uncertainty of ± 3% of data [49].

## 3. Mathematical analysis

The basic mathematical equations are presented in this section for both thermal analysis and energy analysis of the linear Fresnel solar collector used in study.

### 3.1. Thermal analysis

This analysis aims to determine both useful energy and thermal efficiency. Equation (1) gives the useful energy by achieving the energy balance in the volume of water.

$$Q_u = \dot{m}_w C_w (T_{wo} - T_{wi}) \tag{1}$$

where, $Q_u$: useful energy (W), $\dot{m}_w$: water mass flow rate (kg/s), $C_w$: specific heat of water (4.187 kJ/kg.$^o$C), $T_{wo}$& $T_{wi}$: outlet and inlet temperatures of water (°C), respectively.

Equation (2) describes the solar energy available to the collector. It is the product of the beam solar radiation and the aperture area of the collector. The total aperture area of the solar collector considered the projection of the mirrors on the horizontal plane.

$$Q_s = G_b A \tag{2}$$

where, $Q_s$: available solar energy (W), $G_b$: solar beam radiation (W/m$^2$), $A$: aperture area of the collector (m$^2$).

Thermal efficiency ($\eta_{th}$) represents the ratio of useful heat to available solar energy, which can be expressed in Equation (3) [50,51]:

$$\eta_{th} = \frac{Q_u}{Q_s} \tag{3}$$

### 3.2. Exergy analysis

Exergy analysis is a useful method for evaluating solar collectors, especially those operating at medium and high temperature ranges. Exergy is the maximum useful work that can be produced via a flow of energy or substance when it comes to equilibrium with its environment.

The useful exergy rate of a linear Fresnel solar collector used water as working fluid as given by Equation (4) [52,53]:

$$E_u = Q_u - \dot{m}_w C_w T_a \, ln \frac{T_{wo}}{T_{wi}} \tag{4}$$

where, $E_u$: useful exergy rate (W), $T_a$: ambient temperatures (K).

The exergy rate of the available solar energy can be calculated by the Petela model [54]:

$$E_s = Q_s \left[ 1 - \frac{4}{3}\left(\frac{T_a}{T_s}\right) + \frac{1}{3}\left(\frac{T_a}{T_s}\right)^4 \right] \tag{5}$$

where, $E_s$: exergy rate of the available solar energy (W), $T_s$: The sun

**Table 2**
Ranges and uncertainty for measuring devices.

| Device | Range | Uncertainty |
|---|---|---|
| Thermocouples type-K | 0–200 °C | ±0.5 |
| Flow meter | 0–30 l/min | ±0.1 |
| Solar power meter | 0–2000 W/m$^2$ | ±50 |
| Mercury thermometer | 0–100 °C | – |
| Anemometer | 0.4–30 m/s | ±0.02 |

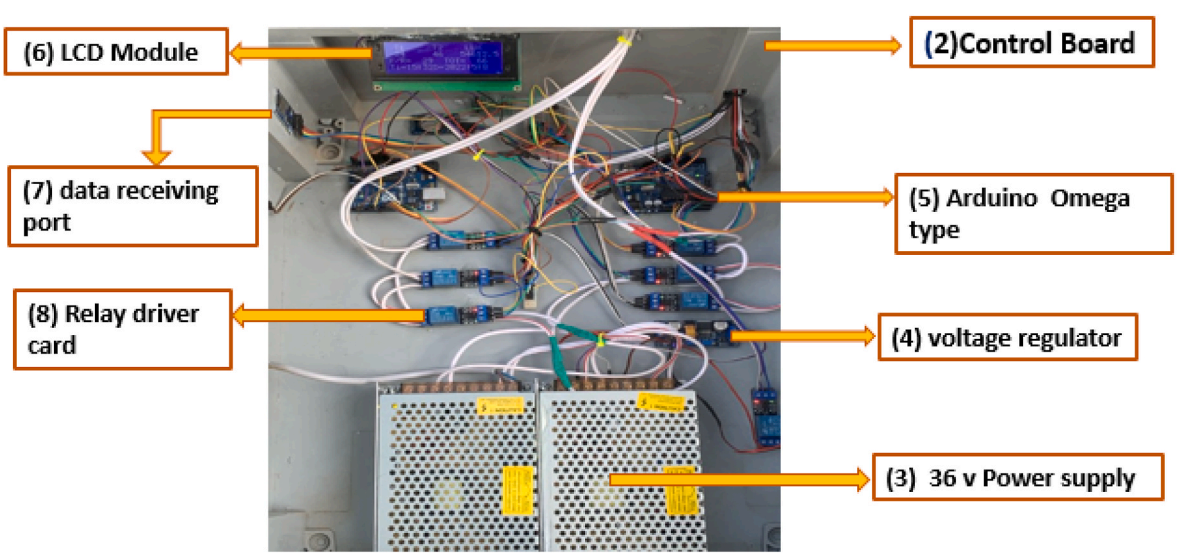


**Figure 5.** Tracking system control board components.


**Figure 6.** Photograph of the linear Fresnel solar collector used in study.

temperature (5770 K) [55].

Exergy efficiency ($\eta_{ex}$) represents the ratio of output exergy rate to input exergy rate, which can be expressed in Equation (6) [52,56]:

$$\eta_{ex} = \frac{E_u}{E_s} \tag{6}$$

### 3.3. Uncertainty analysis

The uncertainty (error) in the experimental tests is evaluated using Equation (7) [57]:

$$e_R = \sqrt{\left(\frac{\partial R}{\partial V_1} e_1\right)^2 + \left(\frac{\partial R}{\partial V_2} e_2\right)^2 + \ldots\ldots + \left(\frac{\partial R}{\partial V_n} e_n\right)^2} \tag{7}$$

The accuracy of this study was deemed acceptable as the measurement uncertainty did not exceed 4 %.

## 4. Numerical simulation

ANSYS FLUENT CFD is used to create a simulation model in order to analyze the water thermal behavior inside the receiver in terms of temperature distribution inside the tube, with assuming that the fluid is 3-D, turbulent, steady state and incompressible.

The governing equations can be described for fluid in the 3-D Cartesian coordinate as follows:

Continuity equation:

$$\frac{\partial(\rho u)}{\partial x} + \frac{\partial(\rho v)}{\partial y} + \frac{\partial(\rho w)}{\partial z} = 0 \tag{8}$$

Momentum equations:

In X-direction:

$$\frac{\partial(\rho u)}{\partial t} + \frac{\partial(\rho uu)}{\partial x} + \frac{\partial(\rho uv)}{\partial y} + \frac{\partial(\rho uw)}{\partial z} = -\frac{\partial p}{\partial x} + \frac{\partial}{\partial x}\left[\mu \frac{\partial u}{\partial x}\right] + \frac{\partial}{\partial y}\left[\mu \frac{\partial u}{\partial y}\right] + \frac{\partial}{\partial z}\left[\mu \frac{\partial u}{\partial z}\right] + \rho g_x \tag{9}$$

In Y-direction:

$$\frac{\partial(\rho v)}{\partial t} + \frac{\partial(\rho vu)}{\partial x} + \frac{\partial(\rho vv)}{\partial y} + \frac{\partial(\rho vw)}{\partial z} = -\frac{\partial p}{\partial y} + \frac{\partial}{\partial x}\left[\mu \frac{\partial v}{\partial x}\right] + \frac{\partial}{\partial y}\left[\mu \frac{\partial v}{\partial y}\right] + \frac{\partial}{\partial z}\left[\mu \frac{\partial v}{\partial z}\right] + \rho g_y \tag{10}$$

In Z-direction:

$$\frac{\partial(\rho w)}{\partial t} + \frac{\partial(\rho wu)}{\partial x} + \frac{\partial(\rho wv)}{\partial y} + \frac{\partial(\rho ww)}{\partial z} = -\frac{\partial p}{\partial z} + \frac{\partial}{\partial x}\left[\mu \frac{\partial w}{\partial x}\right] + \frac{\partial}{\partial y}\left[\mu \frac{\partial w}{\partial y}\right] + \frac{\partial}{\partial z}\left[\mu \frac{\partial w}{\partial z}\right] + \rho g_z \tag{11}$$

Energy equation:

$$\frac{\partial(\rho ucT)}{\partial x} + \frac{\partial(\rho vcT)}{\partial y} + \frac{\partial(\rho wcT)}{\partial z} = \lambda\left(\frac{\partial^2 u}{\partial x^2} + \frac{\partial^2 v}{\partial y^2} + \frac{\partial^2 w}{\partial z^2}\right) \tag{12}$$

The first stage in the analysis is to import the model into the Fluent and the format file that was used is (Parsolid (x-t)). The second stage is the meshing, which is a process that divides the body into small pieces (finite element), and layers have been made with thickness 0.275 mm on the walls of the tube since improving accuracy is required in this area. The number of elements obtained is: (2235497) and the number of nodes is (1458974). The higher the number of elements, the better the accuracy. In this case, it was obtained Skewenss (0.12724), which is excellent, as the closer the Skewenss gets to zero, the better the mesh. Figure (7) shows the obtained meshFollowing completion of the mesh process, the third stage entails naming the inlet and outlet as well as the heating and absorption surfaces (the outer surface of the tube and the surfaces of the mirrors), as illustrated in Figure (8). Finally, the average solar radiation is taken for the first test and the rest of tests was done via radiation model. Boundary conditions are rigorously defined to accurately simulate the fluid flow and thermal dynamics within the computational domain. In the inlet region, a prescribed flow rate of 0.008 kg/s is imposed with different Temperatures, reflecting the volumetric flow entering the system. Additionally, varying solar radiation intensities that correspond to specific dates 10.45 kW/m$^2$ for April 1, 11.13 kW/m$^2$ for April 22, 13.66 kW/m$^2$ for May 8, and 16 kW/m$^2$ for

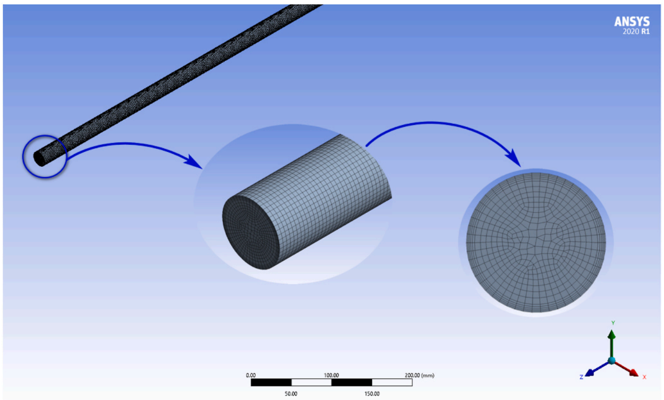


**Figure 7.** Mesh Generation for tube.

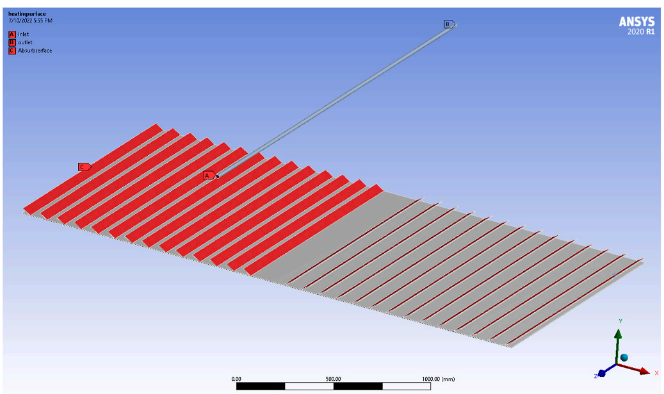


**Figure 8.** Simulation model.

May 27, are applied to represent realistic environmental conditions over the simulation period.

For the outlet region, a condition of outflow is enforced, ensuring the fluid exits the computational domain without any impedance. Notably, the receiving and reflective components of the system remain stationary throughout the simulation. An iteration value of 10,000 is assigned to facilitate convergence, aiming for a Root Mean Square (RMS) residual of 10-4, representing a satisfactory convergence criterion for the computational model.

## 5. Results and discussion

The tests are conducted in the outdoor conditions of the city of Baghdad on four different days and this is the amount of time allotted to experiments. The first and second tests were conducted on April 1 and 22, while the third and fourth tests were conducted on May 8 and 27, respectively. The aim of testing the linear Fresnel solar collector in four time periods is to obtain clear behavior and evaluation for thermal performance. These days were chosen for testing due to the moderate wind speed (less than 2 m/s) and weather fluctuations in terms of clouds and dust, in addition to the time differences that give different thermal perceptions as a result of the difference in insolation and ambient temperatures. The inlet temperature and water flow are approximately constant throughout the test. The inlet temperature is almost settled at 25 °C in the first test, 26.5 °C in the second test, 27 °C in the third test, and 29 °C in the fourth test. While the flow rate is 0.008 kg/s for all tests. The average ambient temperatures during test days are 28.31 °C, 29.13 °C, 29.09 °C, and 34.36 °C on April 1 and 22, May 8 and 27, respectively. Figs. (9)-(12) show the behavior of both the useful energy and the available solar energy to the collector over time for the four

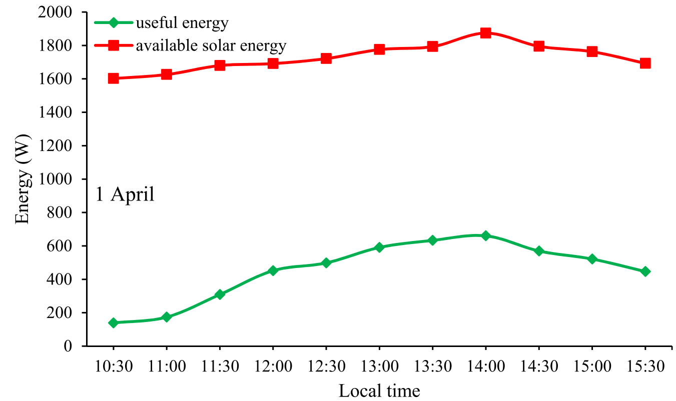


**Figure 9.** The behavior of the useful energy and the available solar energy on April 1.

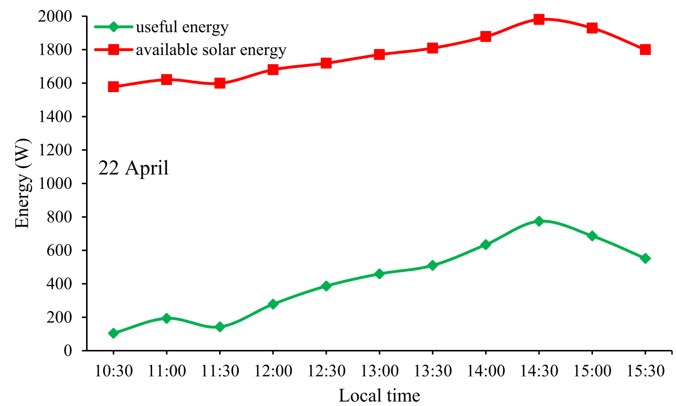


**Figure 10.** The behavior of the useful energy and the available solar energy on April 22.

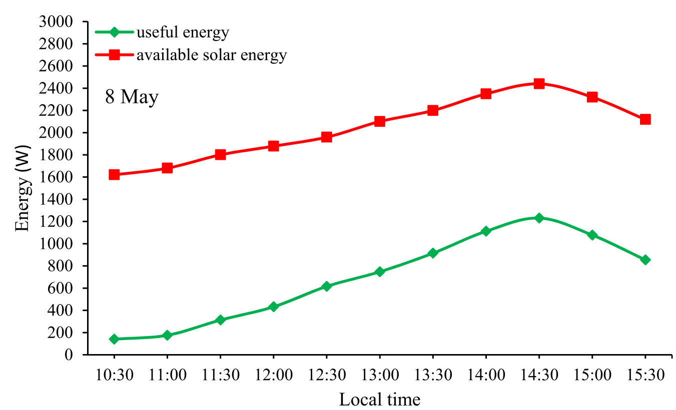


**Figure 11.** The behavior of the useful energy and the available solar energy on May 8.

tests. It is observed for all tests that the behavior of useful energy is directly affected by the available solar energy, as it is directly proportional to it. The reason is mainly due to insolation, which is considered the main influencing parameter for obtaining thermal energy. It is also observed for all tests that the level of useful energy is clearly lower than the level of available solar energy. The reason for this is thermal losses that cannot be reduced according to the second law of thermodynamics, and other thermal losses that can be reduced by passive and active methods.

On April 1, the maximum useful energy is 660.29 W at 14:00, while

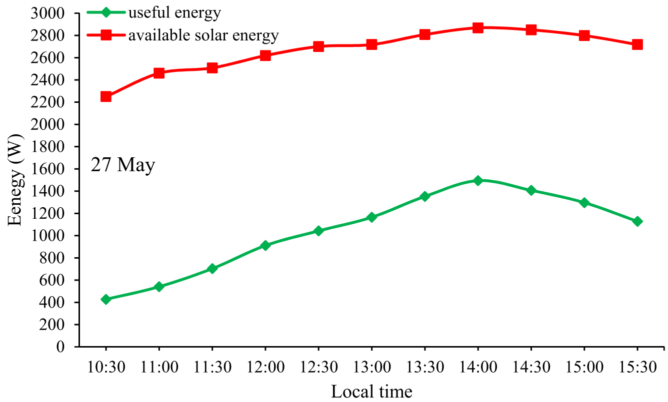


**Figure 12.** The behavior of the useful energy and the available solar energy on May 27.

the average useful energy during the test is 453.90 W. On April 22, the maximum useful energy is 773.76 W at 14:30, while the average useful energy during the test is 429.09 W. On May 8, the maximum useful energy is 1230.98 W at 14:30, while the average useful energy during the test is 692.11 W. On May 27, the maximum useful energy is 1494.34 W at 14:00, while the average useful energy during the test is 1042.61 W. From these results, it is clear that the amount of useful energy increases from April to May, and the reason is due to the increase in insolation from April to May, according to what was reported by Ref. [58]. It should be noted that the reason the average useful energy on April 1 is greater than April 22 is due to weather fluctuations that affected the level of insolation at the beginning of the test on April 22.

Figure (13) shows the behavior of thermal efficiency during the four test periods. This figure is the most important for evaluating the thermal performance of the linear Fresnel solar collector, given that the thermal efficiency shows the way in which the solar collector uses the available solar radiation during test periods, taking into account the optical and thermal losses at the same period. There is a similarity in behavior between thermal efficiency and useful energy. However, it seems that the efficiency curve is more conceptual and comprehensive for evaluating thermal performance because it takes into account the available solar radiation at every moment. With the exception of the test on April 1, the thermal efficiency recorded the highest values during the period from 14:00 to 15:00, and therefore it can be considered that during this period the absorber tube was heated properly. The maximum thermal efficiency reached 35.31 %, 39.08 %, 50.47 %, and 52.10 % on April 1, April 22, May 8, and May 27, respectively. The average thermal efficiency reached 26.26 %, 24.38 %, 33.90 %, and 39.15 % on April 1, April 22, May 8, and May 27, respectively. Thermal efficiency increases from April to May due to the increase in insolation level as mentioned previously.

It should be noted that the thermal efficiency values recorded are considered excellent compared to the values reported in previous studies [32,59] due to the use of the dual-axis tracking system. This makes the application of this type of solar collectors in Baghdad city excellent in terms of performance and obtaining high temperatures, but the costs of construction, operation and maintenance poses challenges that limit its use, especially for domestic purposes.

Figure (14) describes the behavior of exergy efficiency during the four test periods. This parameter is affected by the thermal efficiency, the fluid and ambient temperature level, as well as the insolation level. In general, it can be seen that exergy efficiency levels in May are much higher than in April. The maximum exergy efficiency reached 0.6328 %, 0.8614 %, 2.17 %, and 2.35 % on April 1, April 22, May 8, and May 27, respectively. The average exergy efficiency reached 0.2987 %, 0.3307 %, 1.11 %, and 1.31 % on April 1, April 22, May 8, and May 27, respectively. Generally, the exergy efficiency has low values because of the low operating temperature levels up to 100 °C. It is also noted that the fluctuations in the behavior of energy efficiency are much greater than in thermal efficiency because the non-linear variation of the other parameters (fluid temperature levels, thermal efficiency, and insolation level). It should be noted that improving the exergetic performance reduces irreversibility losses and entropy generation.

Equations for both thermal and exergy efficiency of collector are also obtained based on experimentally measured instantaneous efficiency values, solar radiation, and water and ambient temperatures. This is done through a set of experimental data for one of the test days, which achieves a linear relationship between efficiency VS $\frac{T_{av}-T_a}{G_b}$, as shown in Figures (15) and (16), where the average water temperature $T_{av}$ for inlet and outlet was relied upon as a variable [60].

The relationship between thermal efficiency and $\frac{T_{av}-T_a}{G_b}$ with $R^2 = 0.75$ can be described as follows:

$$\eta_{th} = 0.4233 - 51.795\frac{T_{av} - T_a}{G_b} \tag{13}$$

As $\frac{T_{av}-T_a}{G_b}$ increases from 0.0017 to 0.0056 m$^{2\circ}$C/W, the thermal efficiency values decrease from 33 % to 14 %. This is an indication of an increase in the temperature of the receiver and an increase in heat losses. The intersection with the Y axis represents the optical efficiency of the system, and this indicates the presence of optical losses of about 58 % of the total radiation intercepted by the receiver. This makes it necessary to use techniques other than the finned tube to enhance optical efficiency, such as a cavity receiver.

Also the relationship between exergy efficiency and $\frac{T_{av}-T_a}{G_b}$ with $R^2 = 0.91$ can be described as follows:

$$\eta_{ex} = 0.6715\frac{T_{av} - T_a}{G_b} - 0.0003 \tag{14}$$

Exergy efficiency shows a completely different behavior from

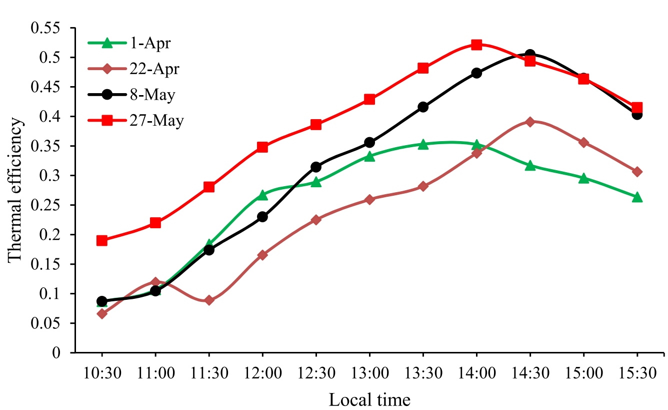


**Figure 13.** The behavior of the thermal efficiency during the four test periods.

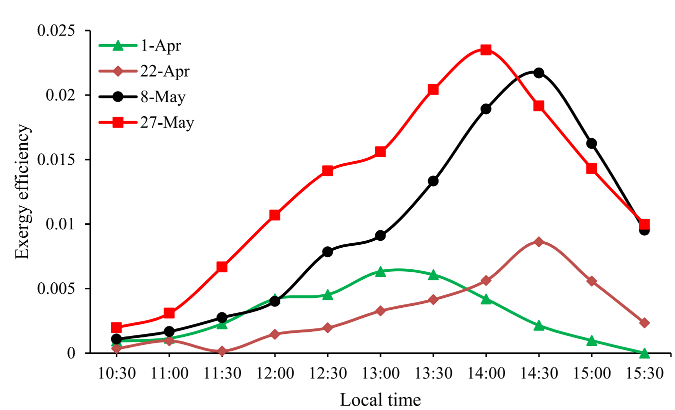


**Figure 14.** The behavior of the exergy efficiency during the four test periods.

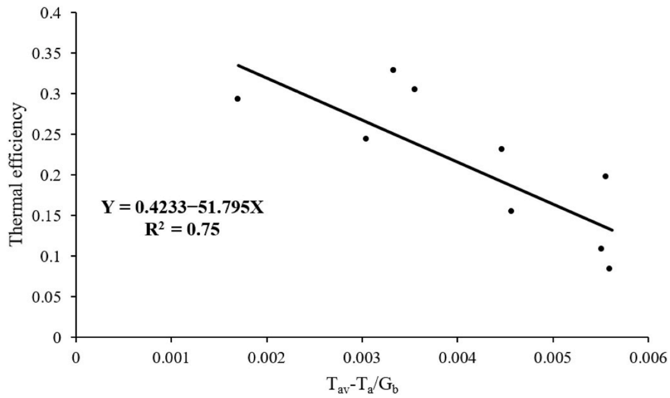


**Figure 15.** Thermal efficiency VS $\frac{T_{av}-T_a}{G_b}$ for system.

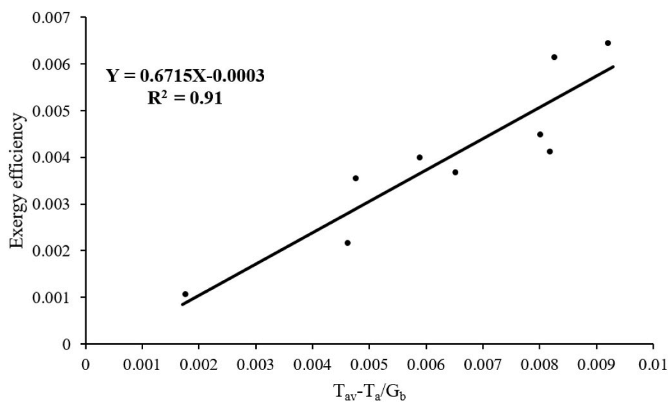


**Figure 16.** Exergy efficiency VS $\frac{T_{av}-T_a}{G_b}$ for system.

thermal efficiency with $\frac{T_{av}-T_a}{G_b}$ as reported in previous studies [32,61].

In order to verify the experimental results, a simulation model of the solar collector is created by CFD, with inlet temperature and water flow similar to what was used in experimental tests. The maximum solar radiation is taken in each test, not the instantaneous solar radiation, to obtain direct simulation results. Figures (17)–(20) show the temperature distribution inside the absorber tube for the four tests. It can be noted that the water temperature is higher on the lower side of absorber tube because this side is most exposed to radiation reflected from the mirror strips. It is also observed that the level of water temperature inside the

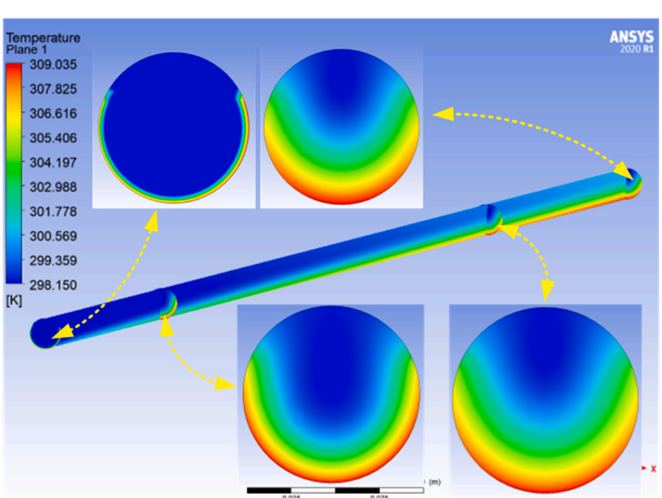


**Figure 17.** Temperature distribution in first test (April 1).

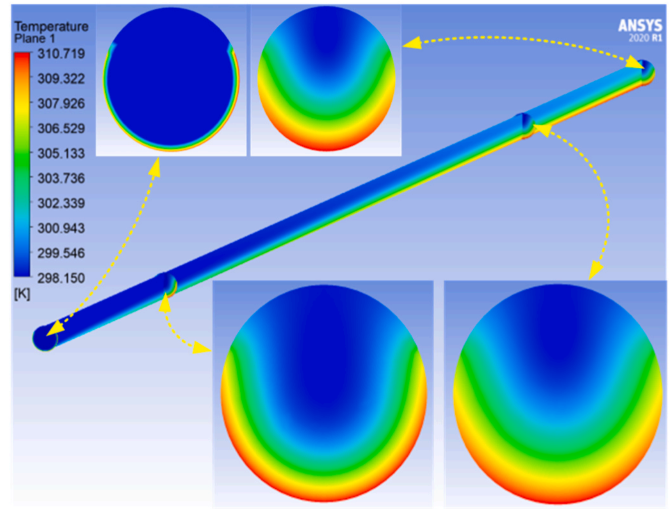


**Figure 18.** Temperature distribution in second test (April 22).

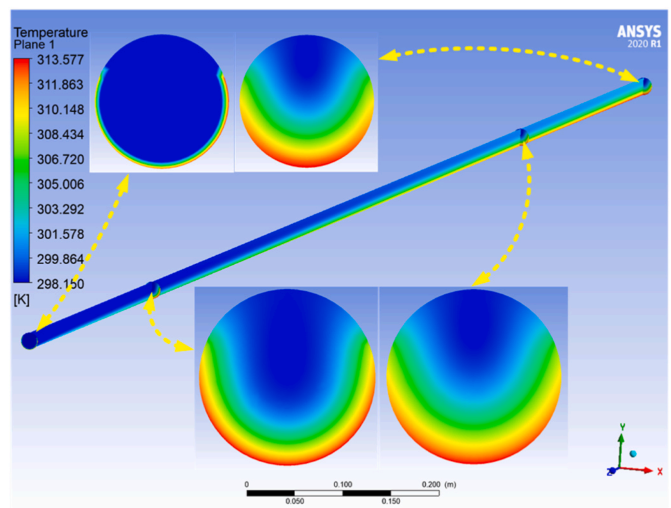


**Figure 19.** Temperature distribution in third test (May 8).

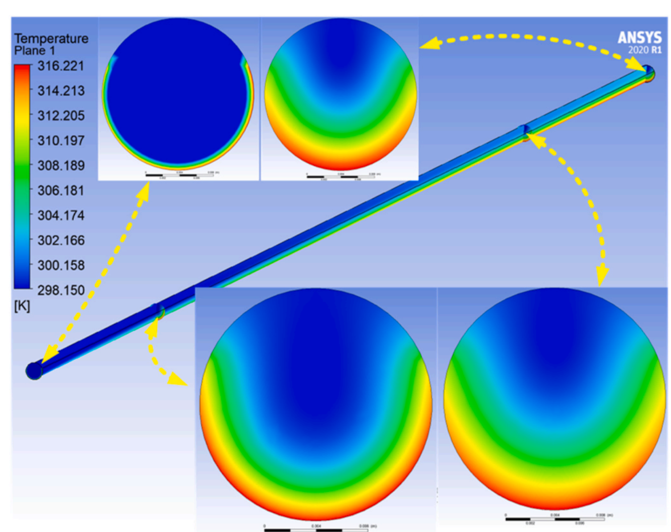


**Figure 20.** Temperature distribution in second test (May 27).

water tube, especially at the outlet, increases from April to May, and this is consistent with the experimental results because increasing the outlet temperature increases the useful energy and thermal efficiency.

## 6. Conclusion

This study evaluated the thermal performance of a linear Fresnel solar collector in the outdoor conditions of Baghdad city by conducting experimental tests utilizing water as the working fluid. Tests were conducted on April 1 and 22, and also on May 8 and 27. Several parameters were considered, most notably useful energy, thermal efficiency, and exergy efficiency. After analyzing the results, it can be said that insolation is the basic parameter in increasing the thermal performance of the solar collector. The average useful energy, thermal efficiency and exergy efficiency increased by 33.59 %, 32.92 %, and 77.20 %, respectively at the test on May 27 compared to April 1 due to the higher insolation level. The validity of the experimental results is confirmed by a brief numerical analysis using CFD. It can be considered that using this type of solar collectors in Baghdad city is excellent in terms of performance and obtaining medium and high temperatures, but costs of construction, operation and maintenance pose challenges that limit its use, especially for domestic purposes. It should be noted that the performance of this type can be further improved in several ways, such as using an evacuated tube instead of a copper tube or using a trapezoidal cavity receiver.

## CRediT authorship contribution statement

**Qusay J. Abdul-Ghafoor:** Writing – review & editing, Writing – original draft, Supervision, Resources, Project administration, Methodology, Funding acquisition. **Sundus Huseein Abed:** Validation, Resources, Project administration, Investigation, Funding acquisition, Data curation. **Saif Ali Kadhim:** Writing – review & editing, Writing – original draft, Methodology, Investigation, Formal analysis, Data curation, Conceptualization. **Mustafa A. Al-Maliki:** Writing – review & editing, Writing – original draft, Software.

## Declaration of competing interest

The authors declare that they have no known competing financial interests or personal relationships that could have appeared to influence the work reported in this paper.

## Data availability

Data will be made available on request.

## References


[1] H.Q. Khafaji, H.A. Abdul Wahhab, W.A.K. Al-Maliki, F. Alobaid, B. Epple, Energy and exergy analysis for single slope passive solar still with different water depth located in Baghdad center, Appl. Sci. 12 (17) (2022) 8561, https://doi.org/10.3390/app12178561.

[2] S. Shanmugan, K.A. Hammoodi, T. Eswarlal, P. Selvaraju, S. Bendoukha, N. Barhoumi, A. Elsheikh, A technical appraisal of solar photovoltaic-integrated single slope single basin solar still for simultaneous energy and water generation, Case Stud. Therm. Eng. 54 (2024) 104032, https://doi.org/10.1016/j.csite.2024.104032.

[3] S.A. Kadhim, A.H. Askar, Evaluation performance of a solar box cooker in Baghdad, Journal of University of Babylon for Engineering Sciences 26 (10) (2018) 208–216.

[4] O.A.A.M. Ibrahim, S.A. Kadhim, H.M. Ali, Enhancement the solar box cooker performance using steel fibers, Heat Transfer 53 (3) (2024) 1660–1684, https://doi.org/10.1002/htj.23008.

[5] H. Krabch, R. Tadili, A. Idrissi, Design, realization and comparison of three passive solar dryers. Orange drying application for the Rabat site (Morocco), Results in Engineering 15 (2022) 100532, https://doi.org/10.1016/j.rineng.2022.100532.

[6] S.A. Mohammed, W.H. Alawee, M.T. Chaichan, A.S. Abdul-Zahra, M.A. Fayad, T. M. Aljuwaya, Optimized solar food dryer with varied air heater designs, Case Stud. Therm. Eng. 53 (2024) 103961, https://doi.org/10.1016/j.csite.2023.103961.

[7] C. Yıldırım, Theoretical investigation of a solar air heater roughened by ribs and grooves, J. Therm. Eng. 4 (1) (2018) 1702–1712, https://doi.org/10.18186/journal-of-thermal-engineering.365713.

[8] D. Kumar, L. Prasad, Augmentation on heat transfer and friction factor in three sides solar air heaters having an arrangement of multi-V and transverse wire roughness on the absorber plate, Int. J. Therm. 24 (2) (2021) 109–117, https://doi.org/10.5541/ijot.796532.

[9] Q.J. Abdul-Ghafou, A.A. Mohammed, S.A. Kadhim, Evaluation of the effect of dusty weather on the performance of flat plate solar collector, Advances in Natural and Applied Sciences 10 (13) (2016) 125–131.

[10] M.G. Ajel, E. Gedik, H.A.A. Wahhab, L.A. Mahdi, M.T. Chaichan, FEXPERIMENTAL investigation OF PV/T solar collector efficiency with spherical-shaped protrusions on the absorber surface, J. Eng. Sci. Technol. 18 (2023) 55–64.

[11] F.L. Rashid, H.S. Aljibori, H.I. Mohammed, A. Ameen, S. Ahmad, M.B.B. Hamida, A.H. Al-Rubaye, Recent advances and developments of the application of hybrid nanofluids in parabolic solar collector energy systems and guidelines for future prospects, Journal of Engineering Research (2024), https://doi.org/10.1016/j.jer.2024.04.023.

[12] C. Sun, M.N. Fares, S.M. Sajadi, Z. Li, D.J. Jasim, K.A. Hammoodi, A.A. Alizadeh, Numerical examination of exergy performance of a hybrid solar system equipped with a sheet-and-sinusoidal tube collector: developing a predictive function using artificial neural network, Case Stud. Therm. Eng. 53 (2024) 103828, https://doi.org/10.1016/j.csite.2023.103828.

[13] P. Scalco, J.B. Copetti, M.H. Macagnan, J.D. de Oliveira, Linear fresnel solar collector concentrator–a review, in: 26 Th ABCM International Congress of Mechanical Engineering, 2021, November. Florianópolis, SC, Brazil.

[14] A. Rovira, R. Barbero, M.J. Montes, R. Abbas, F. Varela, Analysis and comparison of Integrated Solar Combined Cycles using parabolic troughs and linear Fresnel reflectors as concentrating systems, Appl. Energy 162 (2016) 990–1000, https://doi.org/10.1016/j.apenergy.2015.11.001.

[15] R. Singh, *Modelling and Performance Analysis of Linear Fresnel Collector for Process Heat Generation for Ice Cream Factory in Konya* (Master's Thesis, Middle East Technical University, 2017.

[16] A. Sebastián, R. Abbas, M. Valdés, J. Casanova, Innovative thermal storage strategies for Fresnel-based concentrating solar plants with East-West orientation, Appl. Energy 230 (2018) 983–995, https://doi.org/10.1016/j.apenergy.2018.09.034.

[17] A. Barbón, J.A. Sánchez-Rodríguez, L. Bayón, N. Barbón, Development of a fiber daylighting system based on a small scale linear Fresnel reflector: theoretical elements, Appl. Energy 212 (2018) 733–745, https://doi.org/10.1016/j.apenergy.2017.12.071.

[18] P. Dellicompagni, J. Franco, Potential uses of a prototype linear Fresnel concentration system, Renew. Energy 136 (2019) 1044–1054, https://doi.org/10.1016/j.renene.2018.10.005.

[19] A.K. Khlief, W.A.K. Al-Maliki, H.A. Abdul Wahhab, F. Alobaid, B. Epple, A. A. Abtan, Parabolic air collectors with an evacuated tube containing copper tube and spiral strip, and a new cavity receiver: experimental performance analysis, Sustainability 15 (10) (2023) 7926, https://doi.org/10.3390/su15107926.

[20] N. Kincaid, G. Mungas, N. Kramer, M. Wagner, G. Zhu, An optical performance comparison of three concentrating solar power collector designs in linear Fresnel, parabolic trough, and central receiver, Appl. Energy 231 (2018) 1109–1121, https://doi.org/10.1016/j.apenergy.2018.09.153.

[21] M.J. Montes, R. Barbero, R. Abbas, A. Rovira, Performance model and thermal comparison of different alternatives for the Fresnel single-tube receiver, Appl. Therm. Eng. 104 (2016) 162–175, https://doi.org/10.1016/j.applthermaleng.2016.05.015.

[22] S. Balaji, K.S. Reddy, T. Sundararajan, Optical modelling and performance analysis of a solar LFR receiver system with parabolic and involute secondary reflectors, Appl. Energy 179 (2016) 1138–1151, https://doi.org/10.1016/j.apenergy.2016.07.082.

[23] R. Grena, P. Tarquini, Solar linear Fresnel collector using molten nitrates as heat transfer fluid, Energy 36 (2) (2011) 1048–1056, https://doi.org/10.1016/j.energy.2010.12.003.

[24] M. Hack, G. Zhu, T. Wendelin, Evaluation and comparison of an adaptive method technique for improved performance of linear Fresnel secondary designs, Appl. Energy 208 (2017) 1441–1451, https://doi.org/10.1016/j.apenergy.2017.09.009.

[25] M.A. Moghimi, K.J. Craig, J.P. Meyer, Optimization of a trapezoidal cavity absorber for the linear fresnel reflector, Sol. Energy 119 (2015) 343–361, https://doi.org/10.1016/j.solener.2015.07.009.

[26] F. Chen, M. Li, R. Hassanien Emam Hassanien, X. Luo, Y. Hong, Z. Feng, P. Zhang, Study on the optical properties of triangular cavity absorber for parabolic trough solar concentrator, Int. J. Photoenergy 2015 (2015), https://doi.org/10.1155/2015/895946.

[27] A. Barbón, N. Barbón, L. Bayón, J.A. Otero, Optimization of the length and position of the absorber tube in small-scale Linear Fresnel Concentrators, Renew. Energy 99 (2016) 986–995, https://doi.org/10.1016/j.renene.2016.07.070.

[28] E. Bellos, E. Mathioulakis, E. Papanicolaou, V. Belessiotis, Experimental investigation of the daily performance of an integrated linear Fresnel reflector system, Sol. Energy 167 (2018) 220–230, https://doi.org/10.1016/j.solener.2018.04.019.

[29] A. Barbón, J.A. Fernández-Rubiera, L. Martínez-Valledor, A. Pérez-Fernández, L. Bayón, Design and construction of a solar tracking system for small-scale linear Fresnel reflector with three movements, Appl. Energy 285 (2021) 116477, https://doi.org/10.1016/j.apenergy.2021.116477.

[30] G. Morin, J. Dersch, W. Platzer, M. Eck, A. Häberle, Comparison of linear Fresnel and parabolic trough collector power plants, Sol. Energy 86 (1) (2012) 1–12, https://doi.org/10.1016/j.solener.2011.06.020.
[31] Y. Elmaanaoui, D. Saifaoui, Parametric analysis of end loss efficiency in linear Fresnel reflector, in: 2014 International Renewable and Sustainable Energy Conference (IRSEC), IEEE, 2014, October, pp. 104–107, https://doi.org/10.1109/IRSEC.2014.7059813.
[32] E. Bellos, E. Mathioulakis, C. Tzivanidis, V. Belessiotis, K.A. Antonopoulos, Experimental and numerical investigation of a linear Fresnel solar collector with flat plate receiver, Energy Convers. Manag. 130 (2016) 44–59, https://doi.org/10.1016/j.enconman.2016.10.041.
[33] E. Bellos, C. Tzivanidis, Multi-criteria evaluation of a nanofluid-based linear Fresnel solar collector, Sol. Energy 163 (2018) 200–214, https://doi.org/10.1016/j.solener.2018.02.007.
[34] S. Dabiri, E. Khodabandeh, A.K. Poorfar, R. Mashayekhi, D. Toghraie, S.A.A. Zade, Parametric investigation of thermal characteristic in trapezoidal cavity receiver for a linear Fresnel solar collector concentrator, Energy 153 (2018) 17–26, https://doi.org/10.1016/j.energy.2018.04.025.
[35] M. Ghodbane, Z. Said, A.A. Hachicha, B. Boumeddane, Performance assessment of linear Fresnel solar reflector using MWCNTs/DW nanofluids, Renew. Energy 151 (2020) 43–56, https://doi.org/10.1016/j.renene.2019.10.137.
[36] H. Beltagy, The effect of glass on the receiver and the use of two absorber tubes on optical performance of linear fresnel solar concentrators, Energy 224 (2021) 120111, https://doi.org/10.1016/j.energy.2021.120111.
[37] M.J. Montes, R. Abbas, R. Barbero, A. Rovira, A new design of multi-tube receiver for Fresnel technology to increase the thermal performance, Appl. Therm. Eng. 204 (2022) 117970, https://doi.org/10.1016/j.applthermaleng.2021.117970.
[38] H.A. Hasan, J.S. Sherza, A.M. Abed, H. Togun, N. Ben Khedher, K. Sopian, P. Talebizadehsardari, Thermal and flow performance analysis of a concentrated linear Fresnel solar collector with transverse ribs, Front. Chem. 10 (2023) 1074581, https://doi.org/10.3389/fchem.2022.1074581.
[39] Q. Zhang, S. Chen, B. Yuan, L. Huang, Experimental study of linear Fresnel reflection solar concentrating system, Front. Energy Res. 11 (2023) 1268687, https://doi.org/10.3389/fenrg.2023.1268687.
[40] M. Cucumo, V. Ferraro, D. Kaliakatsos, M. Mele, F. Nicoletti, Linear Fresnel Plant with primary reflectors movable around two axes, Adv. Model. Anal. 55 (3) (2018) 99–107, https://doi.org/10.18280/ama_a.550301.
[41] M. Yang, Y. Zhu, R.A. Taylor, End losses minimization of linear Fresnel reflectors with a simple, two-axis mechanical tracking system, Energy Convers. Manag. 161 (2018) 284–293, https://doi.org/10.1016/j.enconman.2018.01.082.
[42] E. Bellos, C. Tzivanidis, M.A. Moghimi, Reducing the optical end losses of a linear Fresnel reflector using novel techniques, Sol. Energy 186 (2019) 247–256, https://doi.org/10.1016/j.solener.2019.05.020.
[43] V. Sharma, J.K. Nayak, S.B. Kedare, Effects of shading and blocking in linear Fresnel reflector field, Sol. Energy 113 (2015) 114–138, https://doi.org/10.1016/j.solener.2014.12.026.
[44] J. Hoffmann, Testing and analysis of low pressure, transparent tube solar receiver for the sunspot cycle, J. Therm. Eng. 3 (3) (2017) 1294–1307.
[45] H. Ajdad, Y. Filali Baba, A. Al Mers, O. Merroun, A. Bouatem, N. Boutammachte, S. Benyakhlef, Thermal and optical efficiency analysis of the linear fresnel concentrator compound parabolic collector receiver, J. Sol. Energy Eng. 140 (5) (2018) 051007, https://doi.org/10.1115/1.4040064.
[46] M.A. Cucumo, V. Ferraro, D. Kaliakatsos, F. Nicoletti, Study of kinematic system for solar tracking of a linear Fresnel plant to reduce end losses, Eur. J. Eng. Educ. 21 (5) (2019) 393–400, https://doi.org/10.18280/ejee.210501.
[47] N. Salehi, A.M. Lavasani, R. Mehdipour, Effect of tube number on critical heat flux and thermal performance in linear Fresnel collector based on direct steam generation, International Journal of Heat and Technology 38 (1) (2020) 223–230, https://doi.org/10.18280/ijht.380124.
[48] M. Ghodbane, E. Bellos, Z. Said, B. Boumeddane, A. Khechekhouche, M. Sheikholeslami, Z.M. Ali, Energy, financial, and environmental investigation of a direct steam production power plant driven by linear fresnel solar reflectors, J. Sol. Energy Eng. 143 (2) (2021) 021008, https://doi.org/10.1115/1.4048158.
[49] K. Lovegrove, W. Stein (Eds.), Concentrating Solar Power Technology: Principles, Developments and Applications, second ed., Woodhead Publishing Series in Energy, 2020.
[50] S.A. Kadhim, O.A.A.M. Ibrahim, Improving the thermal efficiency of flat plate solar collector using nano-fluids as a working fluids: a review, Iraqi Journal of Industrial Research 8 (3) (2021) 49–60, https://doi.org/10.53523/ijoirVol8I3ID86.
[51] O.A.A.M. Ibrahim, S.A. Kadhim, M.K.S. Al-Ghezi, Photovoltaic panels cooling technologies: comprehensive review, Arch. Therm. 44 (4) (2023) 581–617, https://doi.org/10.24425/ather.2023.149720.
[52] T.J. Kotas, The Exergy Method of Thermal Plant Analysis, Paragon Publishing, 2012.
[53] A. Bejan, Advanced Engineering Thermodynamics, John Wiley & Sons, 2016.
[54] R. Petela, N. Enteria, A. Akbarzadeh, Exergy analysis of solar radiation, in: N. Enteria, A. Akbarzadeh (Eds.), Solar Thermal Sciences and Engineering Applications, 2013, https://doi.org/10.1201/b15507 ch. 2.
[55] R. Khatri, R. Goyal, R.K. Sharma, Comparative experimental investigations on a low-cost solar cooker with energy storage materials for sustainable development, Results in Engineering 20 (2023) 101546, https://doi.org/10.1016/j.rineng.2023.101546.
[56] K.A. Hammoodi, H.A. Dhahad, W.H. Alawee, Z.M. Omara, Energy and exergy analysis of pyramid-type solar still coupled with magnetic and electrical effects by using matlab simulation, Frontiers in Heat and Mass Transfer 22 (1) (2024) 217–262, https://doi.org/10.32604/fhmt.2024.047329.
[57] J.P. Holman, Experimental Methods for Engineers, eighth ed., McGraw-Hill Series in Mechanical Engineering, 2011.
[58] S.A. Kadhim, M.K. Al-Ghezi, W.Y. Shehab, Optimum orientation of non-tracking solar applications in Baghdad city, International Journal of Heat and Technology 41 (1) (2023) 125–134, https://doi.org/10.18280/ijht.410113.
[59] S. Perini, X. Tonnellier, P. King, C. Sansom, Theoretical and experimental analysis of an innovative dual-axis tracking linear Fresnel lenses concentrated solar thermal collector, Sol. Energy 153 (2017) 679–690, https://doi.org/10.1016/j.solener.2017.06.010.
[60] M. Lin, K. Sumathy, Y.J. Dai, R.Z. Wang, Y. Chen, Experimental and theoretical analysis on a linear Fresnel reflector solar collector prototype with V-shaped cavity receiver, Appl. Therm. Eng. 51 (1–2) (2013) 963–972, https://doi.org/10.1016/j.applthermaleng.2012.10.050.
[61] E. Mathioulakis, E. Papanicolaou, V. Belessiotis, Optical performance and instantaneous efficiency calculation of linear Fresnel solar collectors, Int. J. Energy Res. 42 (3) (2018) 1247–1261, https://doi.org/10.1002/er.3925.